# Dielectron Attachment and Hydrogen Evolution Reaction in Water Clusters

Robert N. Barnett,[†] Rina Giniger,[‡] Ori Cheshnovsky,[‡] and Uzi Landman*,[†]

[†]School of Physics, Georgia Institute of Technology, Atlanta, Georgia 30332-0430, United States
[‡]School of Chemistry, The Sackler Faculty of Exact Sciences, Tel-Aviv University, 69978, Israel

ABSTRACT: Binding of excess electrons to nanosize water droplets, with a focus on the hitherto largely unexplored properties of doubly-charged clusters, were investigated experimentally using mass spectrometry and theoretically with large-scale first-principles simulations based on spin-density-functional theory, with all the valence electrons (that is, 8e per water molecule) and excess electrons treated quantum mechanically. Singly-charged clusters $(H_2O)_n^{-1}$ were detected for $n = 6 - 250$, and our calculated vertical detachment energies agree with previously measured values in the entire range $15 \leq n \leq 105$, giving a consistent interpretation in terms of internal, surface and diffuse states of the excess electron. Doubly-charged clusters were measured in the range of $83 \leq n \leq 123$, with $(H_2O)_n^{-2}$ clusters found for $83 \leq n < 105$, and mass-shifted peaks corresponding to $(H_2O)_{n-2}(OH^-)_2$ detected for $n \geq 105$. The simulations revealed surface and internal dielectron, e^-_2, localization modes and elucidated the mechanism of the reaction $(H_2O)_n^{-2} \rightarrow (H_2O)_{n-2}(OH^-)_2 + H_2$ (for $n \geq 105$), which was found to occur via concerted approach of a pair of protons belonging to two water molecules located in the first shell of the dielectron internal hydration cavity, culminating in formation of a hydrogen molecule $2H^+ + e^-_2 \rightarrow H_2$. Instability of the dielectron internal localization impedes the reaction for smaller ($n < 105$) doubly-charged clusters.
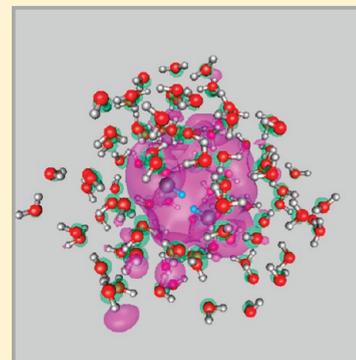
1. INTRODUCTION

The nature and properties of excess electrons in polar fluids (in particular water), both in the bulk as well as in finite aggregates (clusters), have been a subject of intense experimental and theoretical efforts since the discovery of electrons dissolved in ammonia close to 150 years ago[1,2] and the observations close to five decades ago[3,4] about excess electrons generated in aqueous media as a product of water radiolysis. These endeavors, which were often accompanied by lively debates pertaining to the mode of solvation (hydration) of the excess electron, have led to the accumulation of a wealth of information, stimulated significant experimental and theoretical methodological developments, and served as a continuous source of discovery (see recent reviews[5,6]).

The majority of research endeavors (particularly in the context of aqueous systems) addressed the solvation of a single excess electron, which along with its intrinsic relevance as the quintessential simplest quantum mechanical solute appears as an intermediate in numerous charge-induced and charge-transfer chemical and biological processes and plays an important role in radiation physics and biology. Furthermore, starting with the early experiments[7−10] and theoretical[11−13] work in the 1980s and continuing with a recent surge of research activity,[14−20] investigations of excess electron attachment and hydration in water clusters of variable size revealed interesting evolutionary patterns that bridge the finite (molecular) cluster regime with the macroscopic domain. An important advance in understanding the size-dependence of electron hydration phenomena

was derived from the early theoretical predictions[11,12] and related experiments pertaining to the distinction between a surface-bound (SB) excess electron localization mode found for smaller clusters and an interior-bound (IB) hydration for larger clusters. The interplay between the two excess electron localization modes was found in microscopic simulations,[11] as well as modeled through the use of continuum dielectric theory,[12,21] to reflect a size-dependent balance between the energy cost entailed in formation (either in the cluster interior or at the surface region) of a hydration cavity (involving disruption of the hydrogen-bond network) and the gain from attractive charge and dielectric polarization interactions between the excess electron and the hydrating host, with the latter contribution dominating at larger cluster sizes. The size evolution has been predicted[11,12] (and was experimentally measured) to be characterized by a linear approach of the vertical detachment energy (VDE) to the bulk limit (that is, an IB hydrated electron) as $n^{-1/3}$, where n is the number of water molecules in the $(H_2O)_n^{-1}$ cluster; here VDE is the energy required for removal of the excess electron without a change in the nuclear coordinates of the solvent.

While current understanding of the properties of single-hydrated excess electrons, $(e^-)_{aq}$, is rather advanced, though

certain issues remain open (particularly pertaining to the interpretation of the results of photoelectron measurements from singly charges water clusters[5,16−20]), this is not the case for the hydrated dielectron, or $(e^-_2)_{aq}$, consisting of two electrons confined to the same hydration cavity or localized in neighboring ones. Indeed, information about dielectrons in bulk water is rather scant and essentially nonexistent for water clusters (apart from an early single theoretical report[13]). However, for a rather long time the dielectron attracted significant interest as a possible intermediate[22−24] in the bimolecular water reduction reaction (sometime called the hydrogen evolution disproportionation reaction, or hydrated-electron bimolecular self-recombination) discovered about a half a century ago[25−27]

$$(e^-)_{aq} + (e^-)_{aq} \rightarrow H_2 + (2\ OH^-)_{aq} \qquad (1)$$
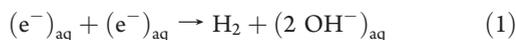
In light of early findings[4,27] that atomic hydrogen is not an intermediate species in the reaction and that spin pairing occurs prior to, or in concert with, the formation of H_2, certain proposed mechanisms for this reaction[24b] involved initial formation of a spin-paired dielectron, $(e^-_2)_{aq}$, that is $(e^-)_{aq} + (e^-)_{aq} \rightarrow (e^-_2)_{aq}$. However, the very existence of $(e^-_2)_{aq}$ has been the topic of contradicting reports; see the experiments in refs 23 and 28 and the theoretical treatments in refs 13 and 29−31. The apparent unsatisfactory state of affairs pertaining to the hydrated dielectron contrasts the rather advanced state of knowledge about dielectron (and higher multielectron) states in condensed media in general (particularly alkali-halide salts[32−36]), and most pertinent to the present study, in other polar liquids, for example, liquid ammonia.[2,30,37]

Here we report on joint experimental and theoretical investigations of the occurrence and nature of doubly-charged water clusters and the dielectron hydrogen evolution (DEHE) reaction $(H_2O)_n^{-2} \rightarrow (H_2O)_{n-2}(OH^-)_2 + H_2$. Key elements of our program are (1) innovative high-resolution gaseous time-of-flight mass spectrometry investigations of the formation of $(H_2O)_n^{-2}$ clusters in the range of $83 \leq n \leq 123$, and, most importantly, measurements of mass signals corresponding to $[(H_2O)_{n-2}(OH^-)_2]$ (for $n \geq 105$) clusters, thus, providing direct evidence about the occurrence of the DEHE reaction, and (2) large-scale first-principles (FP) spin-density-functional-theory (DFT) Born−Oppenheimer molecular dynamics (MD), simulations (FPBOMD) of molecular arrangements, spectra, various modes of excess dielectron binding to water clusters, and of the atomistic mechanism of the DEHE reaction with a focus on $(H_2O)_{105}^{-2}$. In these computations the valence electrons of the water molecules (8 electrons per molecule) as well as the two excess electrons (i.e., a total of 842 electrons in the case of $(H_2O)_{105}^{-2}$)) are treated quantum mechanically. This level of computational complexity and accuracy that we deem essential, reaches well beyond all previous microscopic computational treatments of dielectrons in water[13,31] (as well as all previous computations of large singly-charged water systems[11,12,18]) where only the excess (one or two) electrons were treated quantum mechanically, while the rest of the system (that is, the host water molecules) has been described via model interaction potentials.

The mechanism of the DEHE reaction brought to light by our explorations starts with a concerted approach of two protons from two proximal (reactant) water molecules located in the first (inner) shell of the dielectron hydration cavity (with both excess electrons localized in a common cavity in the interior of the cluster). This process leads to generation of molecular hydrogen,

that is $2H^+ + e^-_2 \rightarrow H_2$, and it is accompanied by (concurrent) proton transfer from neighboring donor water molecules to the two hydroxide residues of the reacting water molecules. A subsequent sequence of proton shuttles (of highly cooperative nature) results in diffusion (and full hydration) of the product hydroxide anions. The DEHE reaction, which is characterized by a rather large computed exothermicity (4.1 eV), entails a calculated (upper bound) activation barrier of 1.8 eV.

The paper is organized as follows. In section 2 we describe the experimental procedure for generation of charged water clusters and the newly constructed high resolution time-of-flight mass spectrometer used in this investigation. Subsequently we give mass spectra showing doubly-charged water clusters with $(H_2O)_n^{-2}$ clusters found for $83 \leq n < 105$, and mass-shifted peaks corresponding to $(H_2O)_{n-2}(OH^-)_2$ detected for $n \geq 105$, thus providing direct evidence about the occurrence of the DEHE reaction. In section 3 we describe our FPBOMD, simulation method, as well as the steered-FPBOMD technique developed by us for explorations of the pathways of the DEHE reaction. We also give (bench-mark) results of our calculations for the neutral monomer, H_2O, and dimer, $(H_2O)_2$ molecules, finding excellent agreement with experimental data for the binding energies, dipole moments, and geometrical parameters. Furthermore, we display our calculated electron vertical detachment energies (VDEs) for water clusters charged by a single excess electron, $(H_2O)_n^{-1}$, $n = 15, 30, 53, 85, 105$, and find that our predicted values compare well, in the entire cluster size range, with values measured in photoelectron experiments.[16b] These results provide a new interpretation of the experimental findings in terms of internal, surface, and diffuse excess electron states in water clusters. Surface and internal modes of attachment of two excess electrons to a water cluster $(H_2O)_{105}^{-2}$ are given in section 4, and the dynamical pathway of the dielectron hydrogen evolution reaction is described in section 4, with a discussion pertaining to the instability of internal localization of dielectrons in doubly-charged water clusters with $n < 105$ water molecules as the origin of the observed impediment of the DEHE reaction in clusters in this size range. We summarize our results in section 6. The appendices give details of the simulation procedure and other pertinent information.

2. EXPERIMENTAL SECTION

In the experiment a wide distribution of water clusters $(H_2O)_n^{-1}$ with $n = 6−250$ is routinely generated using a 10 Hz pulsed nozzle,[38] where neon gas at a pressure of $14−20$ bar is passed into the valve through a water-containing heated reservoir ($50−70$ °C); the reservoir and the corresponding gas lines are thoroughly pumped and baked overnight prior to the experiment. The supersonic expansion is intersected by an electron beam ($40−200$ eV) generating a wide distribution of negatively and positively charged clusters. A newly constructed reflecting time-of-flight mass spectrometer, based on the design in ref 39 with $(m/dm) = 2000$, is used for mass analysis and separation of the clusters. During the extensive expansion conditions and high electron beam currents needed for the doubly-charged cluster generation, the mass peak gets distorted due to the space charge effect, although single hydrogen mass resolution at the relevant mass range is maintained.

When the carrier gas in the expansion is Ar or He, only pristine water clusters are observed in the mass distribution. Occasionally, under favorite expansion conditions, extra argon atoms can be
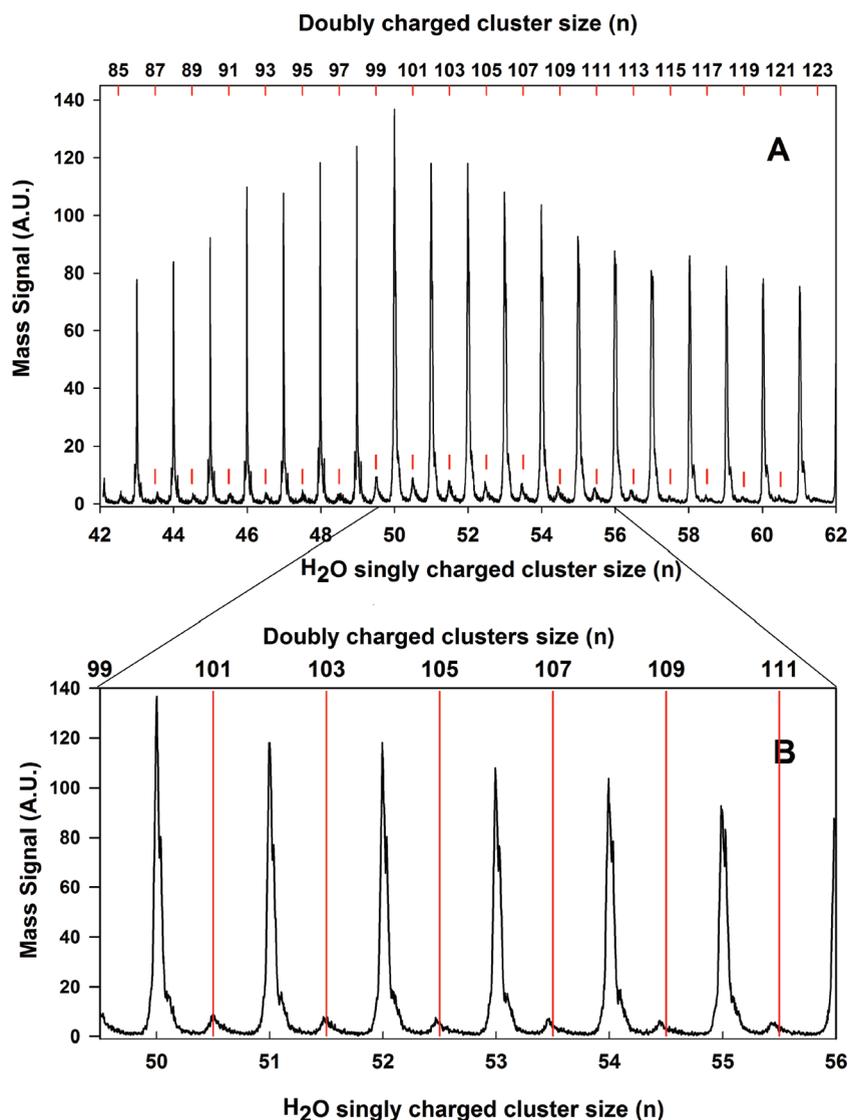
Figure 1. Mass spectrum of negatively charged clusters, produced in the expansion of water vapor in Ne carrier gas. The mass spectra reveal three types of clusters: The large peaks correspond to singly-charged water clusters $(H_2O)_n^{-1}$ (as well as doubly-charged ones with $2n$ water molecules, that is the same mass to charge ratio as the singly-charged clusters with n molecules) in the range of $n = 42-61$. The corresponding mass scale (in water molecule mass units) is given in the bottom axes of panels A and B. The small peaks, situated between the large ones, are attributed to doubly-charged clusters with an odd number of water molecules (the corresponding mass scale given in the top axes). Up to $n = 103$, the locations of the peaks coincide precisely with the anticipated masses indicated by the small vertical red marks in panel A (long thin red bars in B); see for example the locations of the peaks for $(H_2O)_{101}^{-2}$ and $(H_2O)_{103}^{-2}$. At higher masses, corresponding to doubly-charged water molecules $(H_2O)_n^{-2}$ with $n > 103$, the mass values shift down by two atomic mass units, indicating the loss of H_2 due to the occurrence of the dielectron hydrogen-evolution reaction.

attached to the negatively charged water clusters; this indicates that the temperature of the clusters is in the range of several tens degrees Kelvin. No other peaks are discernible in the mass spectrum over the entire mass range. However, when Ne is used as the carrier gas, new peaks are observed in the mass range corresponding to $n = 41-62$, see Figure 1A. Two series of peaks can be clearly distinguished in the mass spectrum: the large ones, which do not depend on the expansion conditions, correspond to singly negatively charged water clusters, and the smaller ones, which appear only under favorable conditions, are assigned to doubly-charged water clusters with an odd number of water molecules; recall that time-of-flight mass spectrometry determines the ions mass-to-charge ratio as they are accelerated in an electric field of known strength.

Note in Figure 1B that, up to $n = 52$, the small peaks coincide precisely with the anticipated mass of $(H_2O)_{2n+1}^{-2}$, as marked by the red (thin) vertical bars. Peaks corresponding to doubly-charged clusters containing 105 water molecules and larger ones exhibit a down-shift, indicating the loss of H_2. These peaks are characterized by a tail extending to higher mass (see below). The mass signals of doubly-charged clusters with an even number of water molecules either coincide with, or are masked by (in case of H_2 loss), the larger signal of the corresponding singly-charged water clusters.

The peaks attributed to $(H_2O)_{2n-1}(OH^-)_2$ (i.e., for $n \geq 52$) originate from the intracluster hydrogen evolution reaction (resulting in H_2 loss) discussed above and not from the presence of impurities (such as OH^- or O^{2-}) in the expansion. In support

Table 1. Calculated and Measured Energies (Atomization Energy, ΔE_a, in eV), Geometrical Parameters (O−H Distance, $d(OH)$, and Intramolecular Angle, $\emptyset(HOH)$), and Dipole Moments, μ (in Debey Unit) of the H_2O Molecule[a]

H_2O	calcd	exp
ΔE_a	9.83 eV	9.51 eV
$d(OH)$	0.97 Å	0.96 Å
$\phi(HOH)$	104.5°	104.5°
μ	1.84 D	1.85 D

[a] Measured geometrical parameters are from Benedict, W. S.; Gailer, N.; Plyer, E. K. *J. Chem. Phys.* **1956**, *24*, 1139, and the experimental dipole moment is from Clough, S. A.; Beers, Y.; Klein, G. P.; Rothman, L. S. *J. Chem. Phys.* **1973**, *59*, 2254. The experimental atomization energy is quoted in Ruscic, B.; Wagner, F. A.; Harding, L. B.; Asher, R. L.; Feller, D.; Dixson, D. A.; Peterson, K. A.; Song, Y.; Qian, X.; Ng, C.-Y.; Liu, J.; Chen, W.; Schwenke, D.W. *J. Phys. Chem. A* **2002**, *106*, 2727.
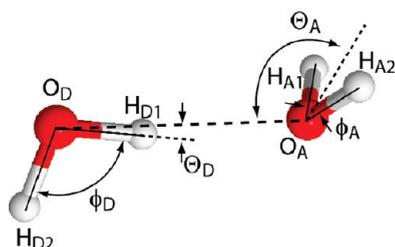
Figure 2. Definition of the geometrical parameters characterizing the water dimer molecule $(H_2O)_2$. For calculated and experimentally measured values see Table 2.

of this conclusion, we note that these extra peaks are not discernible in the mass range smaller than $n = 41$.

While the focus of our study here is on the hydrogen evolution reaction, we remark that the formation mechanism of the doubly-charged water clusters involved in this reaction is likely to proceed through the coalescence of two singly-charged water clusters $(H_2O)_n^{-1}$ rather than the direct attachment of a second excess electron to a singly-charged water cluster, which would be inhibited by the large coulomb barrier. Indeed, according to our calculations, the total energy gain $\Delta E = E[(H_2O)_{52}]^{-1} + E[(H_2O)_{53}]^{-1} - E[(H_2O)_{105}^{-2}(ss')] = 2.85$ eV, which is equivalent to heating of the cluster by 70 K (the heating is likely to be even higher when the translational kinetic energy of the colliding clusters is included); here, $[(H_2O)_{105}^{-2}(ss')]$ denotes an equilibrated 105 molecule doubly-charged cluster with each of the two excess electrons localized in its own "surface cavity" (see the state labeled ss' in Figure 3A, below). Additionally, the above gain in energy upon coalescence implies that, in the range measured here (i.e., $(H_2O)_n^{-2}$ with $n \geq 85$), fission of doubly-charged clusters into two singly-charged fragments is inhibited by a sizable fission barrier.[40]

In our experiment the flight time of clusters from the moment of generation to that of mass analysis is about 400 μs, allowing ample time for the DEHE reaction to occur; our MD simulations indicate that the product H_2 molecule leaves the cluster on a much shorter time-scale. Because the DEHE reaction involves an activation transition state barrier (see below), the reaction time may become comparable to the transit time of the clusters in the acceleration fields of the mass spectrometer. This can give rise to the broadening of the peaks

Table 2. Calculated and Measured Energies (Intermolecular Binding Energy, ΔE_b, in eV), Geometrical Parameters (see Figure 2), and Dipole Moments, μ, in Debey Unit, of the Water Dimer $(H_2O)_2$ Molecule[a]

$(H_2O)_2$	calcd	exp
ΔE_b	0.23 eV	0.236 ± 0.030 eV
$d(O_AH_A)$	0.97 Å	
$\phi_A(H_{A1}O_AH_{A2})$	105.0°	
$d(O_DH_{D1})$	0.98 Å	
$d(O_DH_{D2})$	0.97 Å	
$\phi(H_{D1}O_DH_{D2})$	105.0°	
$d(O_AO_D)$	2.95 Å	2.98 Å
Θ_A	124°	123° ± 10°
$\Theta_D(O_AO_DH_{D1})$	7.0°	6° ± 20°
μ	2.62 D	2.60 D

[a] The experimental values for the geometrical parameters are from Odutolla, J. A.; Dyke, T. R. *J. Chem. Phys.* **1980**, *72*, 5062. The experimental value for the binding energy is from Curtiss, L. A.; Frurip, D. L.; Blander, M. *J. Chem. Phys.* **1979**, *71*, 2703, and it includes a zero-point contribution of 0.080 eV.

attributed to the doubly-charged clusters that underwent the DEHE reaction.

3. THEORY

Aided by algorithmic advances and the availability of modern parallel computers, we have performed a series of challenging first-principles (DFT) computational investigations where, as aforementioned, in addition to the two excess electrons, all the valence electrons were treated quantum mechanically. To this end, we have employed a FPBOMD simulation method[41] that is particularly suitable for investigations of charged systems because it does not employ a supercell (that is, no periodic replication of the ionic system is used). In these calculations, the spin-density-functional Kohn−Sham equations are solved with the use of a plane-wave basis with a 62 Ry cutoff, in conjunction with norm-conserving soft pseudopotentials[42] (with s and p components) for the valence electrons ($8e^-$ per molecule). We employ the generalized gradient approximation (GGA) for exchange and correlation.[43] In dynamical simulations with the FPBOMD method, the KS spin-DFT equations are solved prior to every propagation time-step (0.5 fs) of the nuclei. For details of the preparation of water clusters with excess electrons see Appendix A.

Prior to explorations of dielectrons in water clusters of various sizes and the DEHE reaction, we have investigated several neutral and singly-charged water cluster systems for which experimental data is available. These comparisons allow us to asses the accuracy of our computational method. First we give in Tables 1 and 2, respectively, our computed results for the energy optimized neutral H_2O molecule and the water dimer $(H_2O)_2$ (for earlier calculations performed by us for this system see refs 41, 44, and 45) and compare them with experimentally measured values for binding energies, geometrical parameters, and dipole moments of these systems (see also Figure 2 where the parameters defining the structure of the water dimer are given); for an accumulation of the experimental results for the water monomer and dimer molecules, see ref 46. The high level of agreement between the measured and calculated values, which is evident from the results

Table 3. Calculated and Measured (ref) Vertical Detachment Energies, VDE (in eV), for Single Excess Electrons in Water Clusters $(H_2O)_n^{-1}$ Containing a Variable Number of Water Molecules, n = 15, 30, 53, 85, and 105^a

n [$(H_2O)_n^{-1}$]	VDE calcd (eV)	VDE exp (eV)	
		I	II
15 d	0.5		0.5
15 s	1.1	0.97	
30 d	0.7		0.59
30 s	1.4	1.34	
53 d	1.2		1.0
53 s	1.9	1.8	
53 i	1.8		
85 d	1.3		1.0
85 s	1.9		
85 i	2.1	2.1	
105 d	1.3		1.15
105 s	2.1		
105 i	2.2	2.19	

^{a} In the first column we give the number of molecules in the cluster, n, and the attachment mode of the excess electron to the cluster (determined from the calculations) is denoted by the designations: i, s, and d, which correspond to i, internal localization; s, surface localization, and d, a diffuse state. The values measured in photoelectron experiments are designated according to ref 16 as I, isomer I, and II, isomer II, and they are listed in the same row as the closest calculated value.

in Tables 1 and 2, affirms the accuracy and quantitative reliability of our computations.

Next, we give in Table 3 our computed results for the vertical ionization energies (or vertical detachment energies, VDEs) of singly-charged water clusters, $(H_2O)_n^{-1}$, containing a variable number of water molecules, n = 15, 30, 53, 85, and 105, and compare them with values measured in photoelectron experiments;[16b] for the theoretical method of preparation of the negatively charged clusters, see Appendix A. For every cluster size, the VDE is obtained as the difference between the total energy calculated for the negatively charged cluster $(H_2O)_n^{-1}$ and for the cluster with one less electron (that is, the neutral cluster, $(H_2O)_n$) with the nuclear configuration in the latter kept frozen as in the anion cluster; the calculated results in Table 3 were obtained, for each cluster size, as averages over dynamical first-principles Born—Oppenheimer trajectories (with a duration of up to 3 ps) simulated at a temperature of 250 K.

For each of the clusters, we have attempted to prepare three types of excess electron states: internal (i), surface (s), and diffuse (d); see Appendix A for details. However, for the smallest clusters, with n = 15 and 30 water molecules, the initially prepared internally localized excess electron state converted (during the preparation) into a surface localized one. For n ≥ 53 the internal state (prepared at 250 K) was found to be metastable (with a life time of several ps at 250 K) converting to a diffuse or surface state; cooling to 50 K preserved the prepared internal state. For the cluster with n = 53 we find that the surface and internal excess electron states have almost the same calculated VDE (1.9 eV), while for the larger clusters (with n = 85 and 105) the VDEs of the surface and internal excess electron states are quite similar, with VDE (s) < VDE (i) by about 0.2 eV; images of the wave

functions of the excess electron internal, surface, and diffuse states in $(H_2O)_{105}^{-1}$ are given in Figure 3D—F. The diffuse state for all cluster sizes is characterized by a significantly lower VDE compared to those of the surface and internal states. Also note an apparent reduced sensitivity of the VDEs to cluster size variations for clusters with n ≥ 53 water molecules.

When giving the experimentally measured VDE values, we list them as isomers I and II (see ref 16b) instead of classifying them according to the localization mode (i, s, or d) assigned to them in ref 16b. For every cluster size we list, each measured VDE in the row of the localization mode was found to have the closest calculated value to the experimental one. Throughout the entire range of cluster sizes, we find a rather good correspondence between the measured and calculated values. In all cases, the VDE of isomer II (assigned in ref 16b as a surface bound excess electron) agrees best with the one found in the simulations to correspond to a (weaker bound) diffuse state, while the measured VDE values under the peak assigned in ref 16b as isomer I are found by us to correlate best with the values calculated for both the internal and the surface localization modes of the excess electron.

The most satisfactory level of agreement between the calculated and measured[16b] VDEs found here (for further details see ref 47) for a rather broad range of cluster sizes, 15 ≤ $(H_2O)_n^{-1}$ ≤ 105, has been achieved through first-principles calculations where, in addition to the excess electron, all valence electrons of the water molecules in the cluster are included. These results provide a new, consistent interpretation of the experimental findings[16b] in terms of internal, surface, and diffuse excess electron states in water clusters, and they set a bench-mark for theoretical treatments of excess electrons in water clusters and serve as a firm foundation for the investigations that are the focus of our paper, namely, the nature of excess dielectrons in water clusters and the pathway of the hydrogen evolution reaction.

To explore the dynamical pathway of the DEHE reaction we used our steered FPBOMD (SFPBOMD) simulation method, where the quantum-mechanically calculated Hellmann—Feynman forces that act on the atoms and govern the system's phase-space trajectory on the ground-state (BO) potential energy surface are supplemented by "steering forces" that act (during a prescribed time interval) on a small subset of atoms (four in the present case) in the vicinity of the reaction region, with the purpose of steering the system toward configurations conducive for reaching the reaction transition state barrier. Subsequent to an interval when steering is applied, the steering forces are dropped, and the system is allowed to evolve freely and attempt (spontaneous) crossing into the reaction product basin. When such crossing is successful, the integral that gives the work done by the applied steering forces along the steered particles' trajectories yields the traction transition state activation energy, E_a. If on the other hand the freely evolving system does not cross into the product zone, steering is resumed starting from the point where it was previously stopped, and the process is repeated until the reaction occurs; for further details about the SFPBOMD method, see Appendix B.

4. DIELECTRON ATTACHMENT TO WATER CLUSTERS

First we survey alternative attachment modes of two excess electrons to water clusters, focusing on those that are pertinent for the DEHE reaction; throughout this study we consider only singlet states for the dielectrons (see below). To this aim, we

7382

dx.doi.org/10.1021/jp201560n |*J. Phys. Chem. A* 2011, 115, 7378–7391
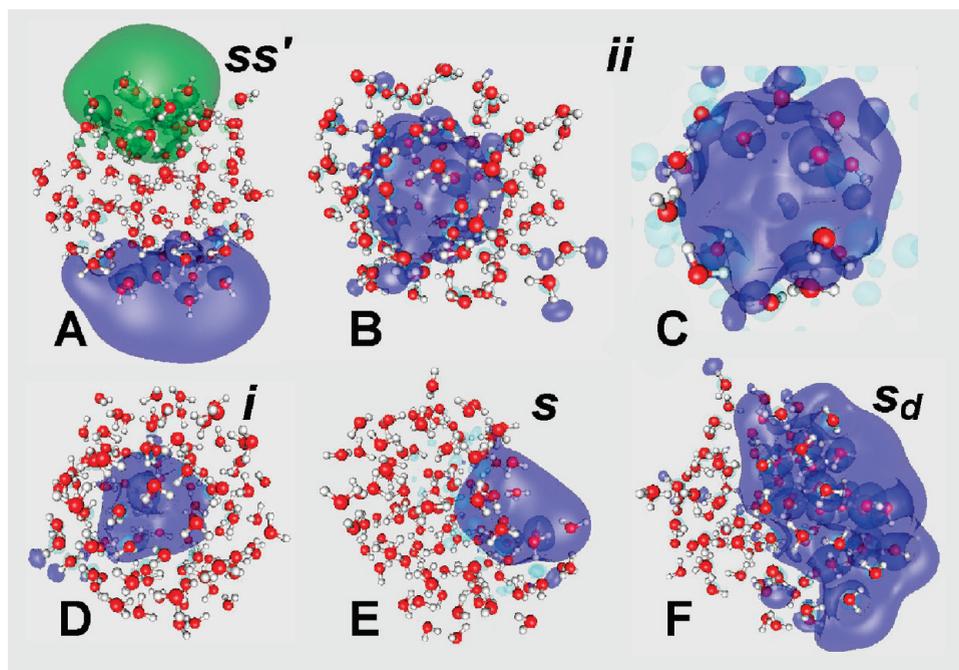
Figure 3. Modes of attachment of two excess electrons (A−C) and a single excess electron (D−F) to a $(H_2O)_{105}$ cluster. In each case an isosurface of the HOKS orbital(s) isosurface(s) encompassing 60% of the electron distribution is depicted, superimposed on the corresponding water molecules' configuration; the oxygen and hydrogen atoms are depicted as red and white spheres, respectively. (A) Two excess electrons localized in separate sites at the surface of the cluster, denoted as (ss'). The two excess electrons occupy different KS orbitals and they have opposite spins. The wave function of the excess electron with the lower energy is depicted in blue. The calculated vertical detachment energies, VDE (1) and VDE (2), are $\langle VDE\,(1)\rangle = 0.03$ eV and $\langle VDE\,(2)\rangle = 1.79$ eV; the gyration radii are $\langle r_e \rangle = 4.8$ and 5.2 Å. (B,C) 2e$^-$ attachment, with both electrons localized internally, denoted as ii. $\langle VDE\,(1)\rangle = 0.11$ eV, $\langle VDE\,(2)\rangle = 2.38$ eV and $\langle r_e \rangle = 5.9$ Å; the asymmetry parameter of the excess electrons distribution (see ref 13) is $\eta = 0.1$, indicating a slightly prolate shape ($\eta = 0$ correspond to a spherical distribution, while positive or negative values correspond to prolate or oblate distributions, respectively). (B) Overall view of the $(H_2O)_{105}{}^{-2}$ cluster. (C) Close-up view of the 16 water molecules in the first (0−4.5 Å, 6 molecules) and second (4.5−5.3 Å, 10 molecules) hydration shells of the internal cavity. (D−F) Single excess electron attachment modes in $(H_2O)_{105}{}^{-1}$, corresponding to the following electron localization patterns: (D) Internal localization (i), with VDE = 2.1 eV, $r_e = 4.3$ Å, and $\eta = 0.11$. The hydration shells are characterized by a first shell, 0−4.25 Å, containing 5.5 molecules, and the second shell, 4.25−5 Å, containing 7.5 molecules. (E) Surface localization (s), with VDE = 1.95 eV, $r_e = 4.3$ Å, $\eta = 0.16$. (F) Diffuse (s_d) state with VDE = 1.28 eV, $r_e = 6.6$ Å. In the above <...> indicates time averaging (see Appendix A).

concentrate on the $(H_2O)_{105}{}^{-2}$ cluster that is the smallest one for which the reaction has been found to occur experimentally (see Figure 1B). For each of the attachment modes that we display, we calculated the vertical detachment energies, VDE (obtained as the difference between the total energies calculated for the original cluster and for the one with one less electron, but without any change in the nuclear configuration between the two charge states). Thus, $VDE(1) = E^{(-1)} - E^{(-2)}$ and $VDE(2) = E^{(0)} - E^{(-1)}$, where $E^{(-m)}$ is the total potential energy of the cluster in charge state m; as aforementioned, both $E^{(0)}$ and $E^{(-1)}$ are calculated for the cluster in the nuclear configuration of the excess dielectron state.

In the attachment mode displayed in Figure 3A, both electrons are surface bound, being localized antipodally with respect to each other (marked ss'). In the ss' configuration, the two excess electrons occupy different KS orbitals and they have opposite spins (i.e., an open shell singlet state). The calculated VDEs for this configuration are $\langle VDE\,(1)\rangle = 0.03$ eV, $\langle VDE\,(2)\rangle = 1.79$ eV. The ss' configuration is characterized by the most favorable enthalpic stability, with $\Delta E_P = 1.3$ eV below the neutral $(H_2O)_{105}$ cluster; ΔE_P is the calculated potential energy difference between the neutral cluster and the doubly negatively charged one. The gyration radii of the two surface-bound excess electrons in the ss' configuration (Figure 3A) are $\langle r_e \rangle = 4.8$ and 5.2 Å, and the distance between the centers of the two excess electron densities

is $d_{ee}(ss') = 15.2$ Å, which is close to the largest possible one because the average diameter of all the $(H_2O)_{105}$ clusters shown in Figure 3 is about 18 Å. The consequent stabilization of this attachment mode is caused by lowering of the interelectron repulsion. Other factors contributing to the enhanced stability of the ss' mode are (a) the smaller disruption of the hydrogen bond network of the cluster associated with electron attachment at two surface cavities (compared to the larger perturbation of the hydrogen-bond network caused by formation of an interior cavity) and (b) the lower electronic kinetic energy of localization, ΔT_L, associated with the two SB excess electrons since each of them is characterized by a more diffuse electron distribution compared to the compact nature of an IB excess electron state (e.g., see the configuration in Figure 3D).

The configuration with both excess electrons sharing an internal hydration cavity (denoted as ii, see Figure 3B,C) is next in order of enthalpic stability. This two-excess electron configuration is stable with respect to the neutral state of the cluster by ≈0.3 eV, with a destabilization energy of up to 1.0 eV from the ss' configuration discussed above. Contributing to the reduced stability of the ii state are the increased repulsion between the two electrons and the increase in ΔT_L caused by the more compact nature of the distributions of the IB electrons. On the other hand, contributing to the stability of the ii configuration are the larger charge and polarization (attractive) interactions

between the compact electron distribution in the cavity ($\langle r_e \rangle$ = 5.9 Å) and the surrounding hydrating water media. The calculated VDEs for the ii configuration are $\langle$VDE (1)$\rangle$ = 0.11 eV and $\langle$VDE (2)$\rangle$ = 2.38 eV.

At finite temperatures,[48] the total potential energies of the two excess electron systems that we discuss here (as well as the energies of the neutral and single excess electron cluster systems that we studied) exhibit large fluctuations. These fluctuations include O—H stretch vibrations, which occur on a ~20 fs time-scale, and larger fluctuations (of the order of ±1.0−1.5 eV at 250 K and ±0.35 eV at 50 K) occurring on a time-scale of ~100 fs; for reference, we recall that the energy of a single hydrogen bond is typically about 0.3−0.4 eV. Molecules near the surface of the cluster make a significant contribution to these large fluctuations. The energies of the KS orbital(s) occupied by the excess electron(s) were found to exhibit much smaller fluctuations (±0.1 eV at 250 K) with no apparent correlation with the large total energy fluctuations noted above. Consequently, we conclude that at finite temperatures it is likely that an ensemble of doubly-charged clusters will be found, made of clusters with different excess electron attachment modes.[49] Moreover, it is likely that double-negatively charged clusters with alternative excess electron attachment modes (e.g., ss', ii, and possibly some higher energy metastable forms[49]) may form through the aforementioned collisional coalescence process of singly-charged clusters (see discussion near the end of section 2); the relaxation of this distribution of clusters to the lowest energy state will depend on the temperature, the thermalization efficiency, and other experimental conditions.

For comparison with the above dielectron states we display in Figure 3D−F atomic configurations of $(H_2O)_{105}{}^{-1}$, with the single excess electron attached internally (i) in (D), on the surface (s) in (E), and in a diffuse state (s_d) in (F); these clusters were prepared as described in Appendix A. The calculated excess electron detachment energy for the s configuration is VDE(s) = 1.95 eV and for the other configurations they are VDE(i) = 2.1 eV and VDE(s_d) = 1.28 eV. As already noted in our discussion pertaining to the results given in Table 3, the calculated values for the internal and surface states of the $(H_2O)_{105}{}^{-1}$ cluster correlate with the photoelectron measured[16b] broad higher energy peak centered at 2.19 eV (for $(H_2O)_{100}{}^{-1}$), and the calculated value for the diffuse state, s_d, correlates with the measured[16b] low-energy data showing a peak centered around 1.15 eV.

5. DIELECTRON HYDROGEN EVOLUTION: REACTION PATHWAY

As a result of our data showing that the DEHE reaction occurs only in clusters $(H_2O)_n{}^{-2}$ with $n \geq 105$ (see Figure 1), we have performed SFPBOMD simulations for a $(H_2O)_{105}{}^{-2}$ cluster, starting from an optimized configuration at 250 K with the two excess electrons localized internally (see the ii configuration, Figure 3B,C). In Figure 4A, we display pertinent distances between atoms participating in the reaction plotted versus time, recorded during the steered reaction-path simulation. In Figure 4B, we show the corresponding time evolution of the eigenvalues of the KS orbitals located at the top of the occupied part of the spectrum of the $(H_2O)_{105}{}^{-2}$ cluster; the highest orbital bound to the water molecules is depicted in blue, and the highest occupied Kohn−Sham orbital (HOKS) that holds the two excess electrons is shown in red (the HOKS orbital maintains its identity as the two-excess-electron-orbital from the start

of the simulation until about t = 400 fs, see below). The vertical (black) dashed lines denote the times t = 375, 410, 425, 440, and 460 fs, corresponding to the selected atomic configurations shown in Figure 4C−G, respectively; pertinent interatomic distances at these times recorded during the SFPBOMD simulation are given in Table 4.

The reaction occurs between two protons with an initial distance d(H−H; t = 0) = 3.87 Å, belonging to two H_2O molecules (located in the dielectron first hydration shell) whose oxygens (marked "1" and "2" in Figure 4D) were separated at the start by d(O−O; t = 0) = 5.27 Å; a view of the system at a slightly later time (375 fs into the SFPBOMD simulation) is shown in Figure 4C along with an isosurface portrait of the internally localized dielectron wave function. The temporal variations of the H−H and O−H distances (the latter starting at d(O−H; t = 0) = 0.99 and 0.97 Å) for the two reacting H_2O molecules are shown in Figure 4A.

The H_2 evolution reaction involves "coalescence" of the two protons (mediated by the internally localized dielectron). This process is found to be correlated with proton transfer from neighboring donor water molecules (marked "d" in Figure 4D−G). The main reaction steps may be described as follows (see interatomic distances in Table 4).

I From the spectral evolution in Figure 4B (see, in particular, the inset) we observe that changes in the eigenvalue spectrum (beyond those resulting from thermal motions of the ions) occur past $t \sim$ 400 fs. At $t \sim$ 410 fs, the eigenvalue energies of occupied electronic states at the top of the spectrum of the H_2O molecules (not including the two excess electrons) begin to rise. These eigenvalues (mainly the top four ones, colored blue and purple) correspond mostly to the sp hybrid orbitals of the two OH bonds (one for each of the reacting H_2O molecules) that stretch as the two reacting hydrogens approach each other. At the same time, the dielectron wave function is seen to remain rather diffuse and nodeless even for the increased interoxygen distance (see Figure 4D corresponding to d(O-(1)−O(2); 410 fs) = 3.64 Å and d(H−H; 410 fs) = 1.28 Å).

II Subsequent evolution of the system is marked by a precipitous decrease of the distance between the two reacting hydrogens (see d(H−H) in Figure 4B, in the time interval between t = 410 fs and 425 fs) and the correlated decrease (i.e., taking a more negative value) of the eigenvalue of the HOKS orbital (colored red in Figure 4A). The atomic configuration at 425 fs shows formation of a hydrogen-like molecule. From the integral of the work done by the steering forces from the beginning of the simulations and up to the point when the steering is stopped and the system is allowed to evolve freely (in the vicinity of the top of the activation barrier, at time t = 412 fs) we estimate an upper bound of the reaction activation barrier of 1.8 eV.

The isosurface of the HOKS orbital shown in Figure 4E (425 fs) exhibits a remarkable 5-center wave function portrait of the dielectron-catalyzed hydrogen evolution reaction. In the central part of the wave function, one observes an embryonic H_2 molecule in the form of two protons (represented by two connected light blue balls) surrounded by a nodeless electron distribution of elliptical shape (colored pink). On each side of this distorted s-like electron distribution one finds p-like wave function components (with positive and negative lobes colored blue and pink) centered on the oxygens (colored green) of the hydroxide (OH$^-$) fragment resulting from the deprotonation

7384

dx.doi.org/10.1021/jp201560n |*J. Phys. Chem. A* 2011, 115, 7378−7391
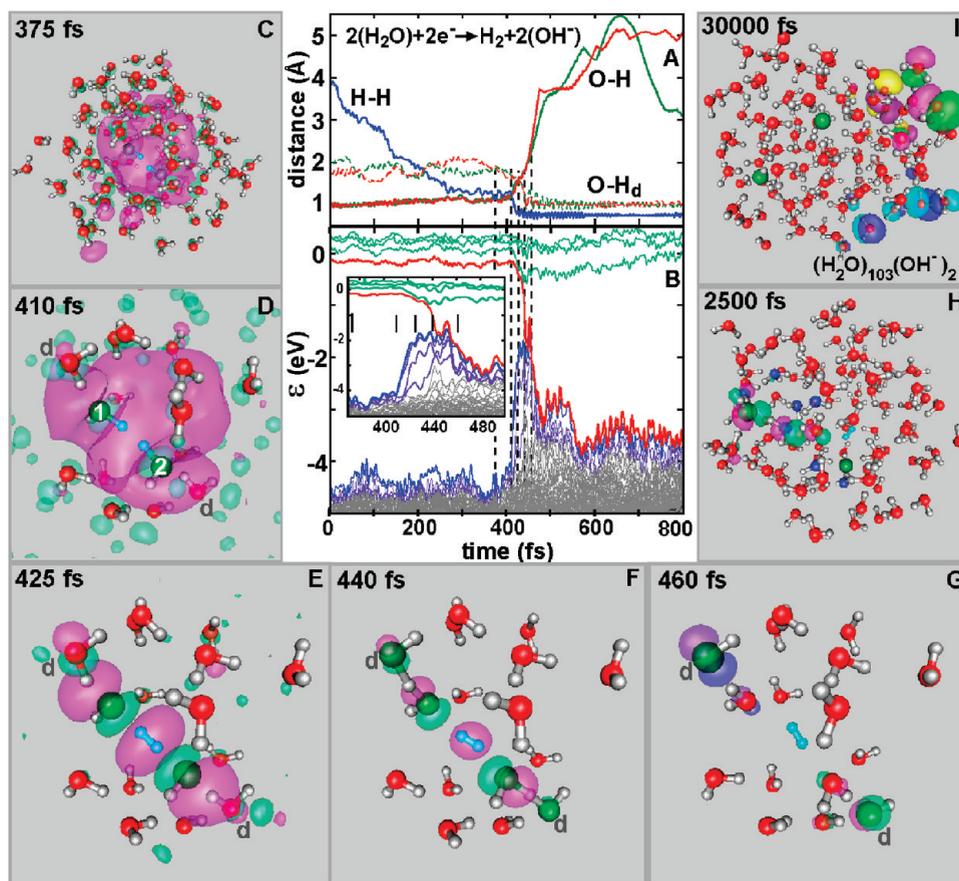
Figure 4. Dielectron hydrogen evolution (DEHE) reaction mechanism in a $(H_2O)_{105}{}^{-2}$ cluster, evaluated with the use of a steered first-principles Born−Oppenheimer molecular dynamics (SFPBOMD) simulation, starting from an equilibrated state of the cluster with an internally localized dielectron in the ii state, see Figure 3B,C. (A) Distances between atoms participating in the reaction plotted versus time (in fs). H−H is the distance between the reacting hydrogens (blue line); for a listing of distances, see Table 4. The distance between the reacting H atom and the O atoms, O−H, in each of the reacting water molecules (marked 1 and 2 in D) are depicted by the red and green lines. The distance between the O atom of the reacting molecule and the proton of a neighboring donor water molecule (marked d in D), O−H_d, is shown for the two reacting molecules and depicted by the dashed red and green lines. (B) Time evolution of the eigenvalues of the KS orbitals of the cluster. The top part of the spectrum (corresponding to orbitals of the water molecules) is depicted by gray lines with the highest water-bound eigenvalue shown in blue. The orbital occupied by the two excess electrons (at the start of the simulation and until $t < 440$ fs) is shown in red; this eigenvalue is separated by an energy gap from the water-bound part of the spectrum until $t < 440$ fs. Unoccupied states (with energies above the excess electron orbital) are shown in green. The vertical (black) dashed lines denote the times $t = 375$, 410, 425, 440, and 460 fs (see also insert in B), corresponding to the selected atomic configurations shown in C−E. (C−E) Atomic configuration and superimposed isosurfaces of the highest occupied KS orbital (HOKS) recorded at the indicated times during the SFPBOMD simulation; the isosurfaces comprise 75% of the electron density, and the purple and green colors of the isosurfaces denote + or − sign of the wave function. For $t = 375$ fs (C), the entire cluster is shown, while for later times (D−G), we zoom in close to the reaction site. Red and small white-gray spheres depict oxygens and hydrogens of H_2O molecules. Oxygens belonging to hydroxide ions are depicted by larger green spheres, and the reacting hydrogens are shown as small blue spheres (shown connected in E−H, corresponding to formation of an H_2 molecule. (H) View of the entire cluster at $t = 2500$ fs, recorded at the end of the SFPBOMD simulation. The two (larger) darker green spheres (the one on the left located at the surface of the cluster) depict the positions of the hydroxide ions at that time, diffusing in the cluster via the proton-transfer assisted diffusion mechanism. Sites that were visited by the hydroxide ions at earlier times of the diffusion trajectory are shown by blue spheres. Isosurface of the HOKS orbital, found to be located on the hydroxide ion near the surface of the cluster (on the left), is shown superimposed on the atomic structure; note that the HOKS is found here to have undergone hybridization with accidentally degenerate orbitals of some neighboring water molecules. (I) Atomic configuration of the $(H_2O)_{103}(OH^-)_2$ cluster, shown with superimposed isosurfaces of the four topmost occupied KS orbitals, each enclosing 80% of the electron density in the corresponding orbital. The distance between the oxygen atoms of the two hydroxide ions is 5.61 Å.

of the two reacting H_2O molecules. At the end of the line connecting the evolving H_2 molecule and resulting hydroxide anions, we find wave function components of p character centered on the two opposing H-donor water molecules (marked "d"). At this time, the proton donation process to the hydroxide fragments is already in progress (see the decrease in the distances $d(O−H_d)$ between the donated protons and the oxygen of the OH^- fragments in Figure 4B;

$d(O(1)−H_d; 425$ fs$) = 1.54$ Å and $d(O(2)−H_d; 425$ fs$) = 1.51$ Å, compared to 1.81 and 1.90 Å at $t = 375$ fs).

III During the following evolution of the system, the O−H bonds stretch further and the H−H bond decreases [see Figure 4B, $d(H−H; 440$ fs$) = 0.74$ Å and $d(O(1,2)−H;$ 440 fs$) = 1.81$ and 1.79 Å, respectively], and concomitantly, we observe the donation of a proton (H_d) to each of the remaining hydroxyl anions from neighboring donor

7385

dx.doi.org/10.1021/jp201560n |*J. Phys. Chem. A* 2011, 115, 7378–7391

Table 4. Interatomic Distances (in Å) Recorded During the SFPBOMD Simulation (Figure 4)[a]

| time	O1−O2	H−H	O1−H	O2−H	O1−Hd	O2−Hd
0	5.27	3.87	0.99	0.97	1.99	1.78
375	3.41	1.18	1.14	1.16	1.81	1.90
410	3.64	1.28	1.19	1.21	1.69	1.61
425	3.83	0.83	1.56	1.61	1.54	1.51
440	4.04	0.74	1.81	1.79	1.25	1.26
460	4.47	0.77	2.41	2.70	0.90	0.98

[a] O1 and O2 are the oxygen atoms of the two reacting water molecules. The reacting hydrogen atoms are denoted as H and the donated hydrogens from the neighboring donor molecules (marked "d" in Figure 4D−G) are denoted as "Hd". Time is in fs.

water molecules (marked d). The coupled OH stretch and proton transfer processes are reflected in the correlated variations of the distances $d(O-H)$ and $d(O-H_d)$ for $t \geq 410$ fs (Figure 4A); see also the corresponding changes in the eigenvalue spectrum in Figure 4B and, in particular, the disappearance of the occupied excess dielectron state upon formation of the H_2 molecule. The H_2 formation process, which is signaled by a sharp drop in the energy of the HOKS (see red curve in Figure 4B in the interval between 225 and 240 fs) and, afterward, is accompanied by enhanced localization of the HOKS wave function components on the better-defined fragments (see Figure 4D) and advancement of the proton donation process.

IV The H_2 formation and proton transfer processes come essentially to completion at $t = 460$ fs, see Figure 4E, where $d(O-O) = 4.47$ Å, $d(H-H) = 0.77$ Å, $d(O(1)1-H) = 2.41$ Å, $d(O(2)-H) = 2.70$, Å . In addition, at this time, the original hydroxide fragments transformed into water molecules, while the donor water molecules (marked "d") converted into hydroxide anions (with their oxygen atoms marked green in Figure 4G (460 fs). This illustrates a step in the proton-transfer mediated diffusion (termed also "structural diffusion"[50]) of the hydroxide anions in the hydration environment of the cluster.

V The hydroxide migration process continues, as illustrated in Figure 4H (2500 fs), where the positions of the OH⁻ anions at this later time are denoted by larger dark green balls separated by 4.08 Å (with the water cluster radius estimated, for reference, to be about 8.75 Å at this time).

It is interesting to note that as the reaction process approaches completion (e.g., 460 fs), the KS orbitals at the top of the occupied electronic spectrum are found on the two O(d)H⁻ anions, which are nearest-neighbors to the two originally reacting water molecules (see the p-like components on the oxygens marked "d" in Figure 4G). As seen from Figure 4B at $t = 460$ fs, the highest occupied eigenvalue (which may be traced back to the dielectron state) starts to merge with the dense eigenvalue manifold of the water cluster, and through mixing between these states it "loses its original identity" as the excess dielectron wave function. In fact, the reason that the p-like orbitals of the OH⁻ anions are still found at the top of the electronically occupied spectrum of the cluster is that their hydration process has not been completed yet.

Even after 2500 fs (Figure 4H and Figure 5A) the p-orbital of one of the hydroxides is found at the top of the spectrum of the $(H_2O)_{103}(OH^-)_2$ H_2 cluster. This is seen for the OH⁻ anion,
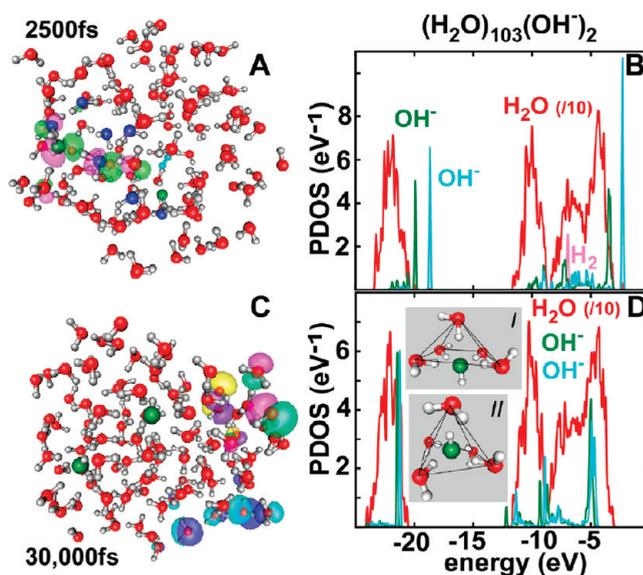
Figure 5. Cluster configurations and projected densities of states, recorded at (A, B) $t = 2500$ fs (that is, at the end of the FPBOMD simulation) and (C, D) after an additional 30 ps of classical MD simulation at 250 K, cooling to 50 K and further FPBOMD evolution (see Appendix B). The cluster configurations given in (A) and (C) are the same as those displayed in Figure 4H and I, respectively, and in addition to the atomic positions, they show (superimposed) the isosurfaces of the highest occupied KS orbitals. The projected densities of states (PDOS) in (B) were evaluated (separately) for the water molecules (in red), hydroxides (in light blue and green) and the H_2 molecule (pink line, only seen in B because the hydrogen molecule evaporated from the cluster at a later time), in the $(H_2O)_{103}(OH^-)_2$ H_2 cluster at $t = 2500$ fs. The PDOS for the $(H_2O)_{103}(OH^-)_2$ shown in D includes in the inset the two main hydration structures of the hydroxide ions. For orbital assignment of the spectral regions in B and D, see text, and Appendix A.

which is located at that time at the surface of the cluster (represented by the darker green ball at the surface of the cluster on the left in Figure 4H or 5A), being hydrated in a plane formed by only 3 H_2O molecules, while full hydration of a hydroxide anion involves a first solvation shell with 4 or 5 H_2O molecules,[50,51] see inset in Figure 5D and ref [52] for geometrical details; note also some contribution of this p-like wave function on neighboring surface water molecules due to orbital hybridization caused by accidental degeneracy. The incomplete hydration of this hydroxide ion is also manifested by the narrow peak (light blue, on line) at ∼−2.2 eV in the projected density of states, PDOS, in Figure 5B, whose energy is higher (less negative) than all other states of the cluster at that time. At the same time, the states of the other hydroxide anion (represented in Figure 4H or 5A, by the dark green ball below the center of the cluster), which has achieved a more complete hydrated state, are found to have lower (more negative and, thus, stronger bound) energies; note the sharp peak (colored green online) at ∼−3.75 eV in the PDOS shown in Figure 5B, which essentially coincides at that time with the top of the spectrum of the water molecules of the cluster (colored red online). For classification and characterization of the electronic states of OH⁻ and H_2O, see Appendix C.

At later times in the cluster evolution internal equilibrium is achieved, see a configuration of the $(H_2O)_{103}(OH^-)_2$ cluster shown in Figure 4I (also Figure 5C), selected from an ensemble

7386

dx.doi.org/10.1021/jp201560n |J. Phys. Chem. A 2011, 115, 7378–7391

simulated with the use of classical and subsequent first-principles quantum simulations (see Appendix D). The isosurfaces shown in Figure 4I (also Figure 5C) correspond to the four HOKS orbitals of the cluster that were found to be localized on under-coordinated water molecules at the surface of the cluster, rather than on the hydrated hydroxide anions, which are found to be fully hydrated. Indeed, examination of the PDOS at this later time (Figure 5D) shows that the top of the spectrum of the cluster consists of states of the water molecules (in particular, those at the cluster surface) and that, upon better hydration, the entire spectrum of the hydroxide anion shifted downward, with the higher-energy states of the hydrated hydroxides anions decreasing in energy from about −2.2 eV in Figure 5B to −5 eV (see sharp peaks in Figure 5D, colored blue and green, corresponding to the two hydroxide anions); for a detailed discussion of the electronic states, see Appendix C.

The calculated equilibrium solvation energy of the $2(OH^-)$ ions in the cluster is 8.95 eV (that is 4.48 eV per ion), in agreement with the range of values deduced from experiments (3.9^{53a} to $4.6 \, eV^{53b}$) and with quantum chemistry calculations[51a] for bulk water. Further analysis of the $(H_2O)_{103}(OH^-)_2$ reveals preferential hydration of the hydroxide ions (separated by 5.6 Å) near the surface of the cluster.[54] The first electron vertical detachment energy from the $(H_2O)_{103}(OH^-)_2$ cluster is VDE-(1) = 4.56 eV, and the second electron detachment energy is VDE(2) = 6.65 eV. Both detachment energies correspond to removal of electrons from water molecules residing at the surface of the cluster, rather than from the hydroxide anions whose electrons are bound more strongly.

From the difference between the potential energy of the equilibrated starting configuration of the doubly-charged cluster $(H_2O)_{105}{}^{-2}$ (with the dielectron localized internally in an ii state) and the energy of the equilibrated product cluster $(H_2O)_{103}(OH^-)_2$ plus that of H_2, we estimate that the exothemicity of the DEHE reaction is 4.1 eV.

To conclude, we address the experimentally observed dependence of the DEHE reaction on the size of the doubly-charged water clusters, with only $(H_2O)_n{}^{-2}$ clusters with $n \geq 105$ (see Figure 1) showing H_2 loss, while the binding of two electrons is observed already for clusters with 83 water molecules. The reaction mechanism that we have explored above requires localization (at least temporarily) of the two excess electrons in a common cavity. Because the only compact dielectron state with both electrons sharing a common cavity is the ii state (that is, dielectron localization in an internal cluster cavity, see Figure 3B,C), we enquire about the cluster-size dependence of the likelihood of finding this dielectron configuration. As aforementioned, for $(H_2O)_{105}{}^{-2}$ (and for larger clusters), the two most stable dielectron configurations are ss′ and ii with both modes having vertical detachment energies $(VDE(j), j = 1,2)$ that correspond to a stable doubly-charged cluster (see caption to Figure 1). Furthermore, the total energy difference between the two dielectron localization modes in the $(H_2O)_{105}{}^{-2}$ cluster was found to be small enough to allow for coexistence of the two attachment modes, thus, enabling initiation of the hydrogen evolution reaction.

In contrast, for a smaller doubly-charged cluster, $(H_2O)_{85}{}^{-2}$, we find that the internal localization mode (ii), is significantly unstable (by 0.5 eV) with respect to the neutral cluster (as well as being unstable, by 1.5 eV, with respect to $(H_2O)_{85}{}^{-1}$), thus, inhibiting its formation. On the other hand, we find that the surface, ss′, dielectron attachment in $(H_2O)_{85}{}^{-2}$ is stable with respect to the neutral (by at least one eV), with a first electron

vertical detachment energy $VDE(1,ss') = 0.1$ eV and $VDE(2; ss') = 1.80$ eV. Consequently, we conclude that while stable doubly negatively charged water clusters $(H_2O)_n{}^{-2}$ may form for $n \geq 83$, the larger instability of the internal excess electron state (e.g., $(H_2O)_{85}{}^{-2}(ii)$) would act to impede the DEHE reaction in clusters of smaller size (i.e., $(H_2O)_n{}^{-2}$, $n < 105$), in agreement with the experimental findings (see Figure 1).

6. SUMMARY

In this paper we presented joint experimental and theoretical explorations of the properties and reaction pathways of excess electrons in a polar medium, with a focus on dielectrons in water clusters, that is $(H_2O)_n{}^{-2}$, which may be viewed as the simplest multiparticle quantum-mechanical solvation (hydration) system. We aimed at determining the critical size at which doubly negatively charged water clusters would appear as stable entities and at understanding the various dielectron attachment and localization modes. Particular emphasize of our investigation has been placed on the following: (i) Detection of mass-spectrometric signatures that signal the occurrence of the bimolecular water reduction reaction (see eq 1), termed here, dielectron hydrogen evolution reaction (DEHE), $(H_2O)_n{}^{-2} \rightarrow (H_2O)_{n-2}(OH^-)_2 + H_2$, whose detection until now has been made only in bulk aqueous media. (ii) Gaining deep insights into the microscopic pathways of the DEHE water splitting reaction, whose mechanism remained hitherto uncertain.

To these aims, we have performed high-resolution time-of-flight mass spectrometry measurements in conjunction with large-scale first-principles density-functional-theory quantum molecular dynamics simulations where, in addition to the excess electrons, the valence electron of the water molecules (eight electrons for each molecule) are treated quantum mechanically. Bench-mark calculations using our FPBOMD method[41] for neutral water monomer and dimer molecules yielded a high level of agreement with experiments (Tables 1 and 2). Moreover, the values calculated by us (Table 3) for the vertical detachment energies of excess electrons from singly negatively charged water clusters, $(H_2O)_n{}^{-1}$ ($n = 15, 30, 53, 85, 105$), compare well with those obtained from photoelectron measurements,[16b] and analysis of the results of these calculations provides a new, consistent, interpretation of the experiments in terms of internal, surface, and diffuse modes of single excess electron attachment to water clusters.

The main findings of our investigations pertaining to dielectrons in water clusters may be summarized as follows:

A Singly-charged water clusters $(H_2O)_n{}^{-1}$ were detected for $n = 6 - 250$. Doubly-charged clusters were measured in the range of $83 \leq n \leq 123$ (Figure 1A) with $(H_2O)_n{}^{-2}$ clusters found for $83 \leq n < 105$, and mass-shifted peaks corresponding to $(H_2O)_{n-2}(OH^-)_2$ detected for $n \geq 105$, thus, providing direct evidence about the occurrence of the DEHE reaction (Figure 1B).

B First-principles (FP) density-functional-theory (DFT) Born−Oppenheimer (BO) molecular dynamics (MD) simulations (FPBOMD) of various modes of excess dielectron binding to water clusters were performed, focusing on $(H_2O)_{105}{}^{-2}$ that marks the onset cluster size for which the DEHE reaction occurs. From the various modes of dielectron attachment that have been explored in these simulations, the favored one has both electrons localized at (antipodal) surface sites (see ss′ configuration in Figure 3A), with the closest dielectron isomer being the

localization mode where both electrons occupy an internal cavity (see ii configuration in Figure 3B,C). The first vertical detachment energies, VDE(1), for both dielectron localization modes are small ($\sim$0.1 eV) due to the repulsion between the two excess electrons. On the other hand, the second vertical detachment energy (that is, second ionization that takes place subsequent to detachment of one of the excess electron, with no interim molecular cluster relaxation) is significantly larger: VDE(2, ss') = 1.79 eV and VDE(2, ii) = 2.38 eV.

C Steered FPBOMD simulations revealed that starting from a dielectron configuration with both electrons localized in an internal cavity (that is, an ii mode), initiation of the DEHE reaction entails concerted approach of two protons from two proximal (reactant) water molecules located in the first (inner) shell of the dielectron hydration cavity. This process leads to generation of molecular hydrogen, that is $2H_2O + e^-_2 \rightarrow 2OH^- + H_2$, and it is accompanied by (concurrent) proton transfer from neighboring donor water molecules to the two hydroxide residues of the reacting water molecules (Figure 4). A subsequent sequence of proton shuttles (of highly cooperative nature) results in diffusion (and full hydration) of the product hydroxide anions (Figures 4 and 5).

D The observed inhibition of the DEHE reaction for $(H_2O)_n^{-2}$ clusters with n < 105, is attributed to the instability of the dielectron internal localization mode (ii) for clusters in this size range.

■ APPENDIX A: PREPARATION OF CHARGED WATER CLUSTERS: THEORETICAL SIMULATIONS OF EXCESS ELECTRON STATES

The excess electron states in singly- and doubly-charged water clusters were simulated using the following procedure:

1) First, to simulate a charged cluster with n water molecules, an approximately spherical water cluster with n + 1 water molecules was prepared and allowed to evolve for 50 ps at 250 K with the use of the TIP3P model potentials[55] (as implemented in the CHARMM force field[56]). Subsequently, for preparation of an interior localized state, a water molecule near the center of the cluster was replaced by a chlorine anion, Cl$^-$, whose interaction with the water molecules was described by the Amber empirical force field.[57] In the Lennard-Jones (LJ) term of this interaction potential, $V(r) = (A/r)^{12} - (B/r)^6$, the Amber A and B coefficients were replaced by (a) $A' = 1.3A$, $B' = 1.3B$ for simulations of a water cluster with a single excess electron, and (b) $A' = 1.6A$, $B' = 1.6B$ for simulations of a water cluster with two excess electrons.

For simulations of an excess electron surface state, a similar procedure was used but for an n water molecule cluster, and at the end of the initial 50 ps MD simulation, a Cl$^-$ ion (with the above modifications of the A and B coefficients) was placed at the surface of the cluster with a distance of 2.5 Å from the nearest oxygen of a surface water molecule. For simulation of the ss' configuration (Figure 3A), two such (modified) Cl$^-$ ions were placed on opposite poles of the water cluster.

(2) The water cluster with the added Cl$^-$ ion(s) was allowed to evolve at 250 K using classical MD for about 25−50 ps.

(3) The (auxiliary) Cl$^-$ ion(s) was replaced by an electron (or two electrons in case of doubly negatively charged clusters), and the system was evolved at 250 K for a time period of up to 1.0 ps using FPBOMD.[41]

(4) The system was cooled to 50 K (using stochastic temperature control of the ionic degrees of freedom, see ref [41]) over a period of 0.25−0.5 ps, and allowed to evolve at 50 K for up to 5 ps.

The "diffuse state", S_d, of the singly-charged $(H_2O)_{105}^{-1}$ cluster (see Figure 3F) resulted from adding a single electron to a previously prepared and equilibrated neutral cluster (that is, without the use of an auxiliary Cl$^-$). The configuration in Figure 3F was obtained from one that was evolved with FPBOMD at 100 K for 2.2 ps, cooled to 50 K in 0.25 ps, and further evolved at 50 K for an additional 2 ps time interval.

■ APPENDIX B: STEERED FIRST-PRINCIPLES BORN−OPPENHEIMER MOLECULAR DYNAMICS (SFPBOMD) SIMULATIONS

The reaction that we wish to simulate takes place in the cluster environment, and stoichiometrically, it may be expressed as

$$2(H_2O) + 2(e^-) \rightarrow 2(OH^-) + H_2$$
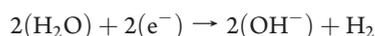
The reaction is assumed to start from the an internal dielectron cluster configuration (that is, state ii depicted in Figure 3B, C). In the present simulation, we assume a temperature of 250 K. We define two time-dependent "steering-potentials", $E_{O-H}(t)$ and $E_{H-H}(t)$, which are included in the equations of motion (see description of the FPBOMD in ref [41]) of the nuclei of the two selected reacting water molecules:

$$E_{O-H}(t) = C_{O-H}\{\min[0, d_{O-H}(t) - D_{O-H}(t)]\}^2/2$$

with

$$D_{O-H}(t) = \min[1.45, 0.82 + 0.0042t]$$

and

$$E_{H-H}(t) = C_{H-H}\{\max[0, d_{H-H}(t) - D_{H-H}(t)]\}^2/2$$

$$D_{H-H}(t) = \max[1.06, 3.6 - 0.085t]$$

Energy is expressed in unit of eV, distance in Å, and time is in fs; $d_{O-H}(t)$ is the distance (obtained from the steered MD simulation at time t) between the oxygen atom and the reacting proton; E_{O-H} is applied to each of the reacting water molecules, with $d_{H-H}(t)$ being the distance (at time t) between the two reacting protons (that is, the ones that eventually would form, with the dielectron, the product hydrogen molecule). The constants in the above equations, $C_{O-H} = C_{H-H} = 9.7$ eV/Å^2, are chosen to take a value equal be about half of the O−H bond spring constant of an H$_2$O molecule in liquid water.

The steering-potential functions were chosen to bring the system to a point near the top of the barrier (as determined in preliminary runs) and to let the system evolve with the stretched O−H and compressed H−H distances until fluctuations and relaxation of solvating neighboring molecules get it over the barrier (which occurred at time t = 412 fs, see Figures 4A and 6). Subsequently, the system evolves dynamically without any steering potentials.

The barrier is estimated as the work done by the steering-potential forces. This work is the integral of $F(t) \cdot v(t)dt$, where v is the particle velocity and F is the applied force obtained (as a derivative) from the steering potential. The integration is taken from the start of the steering simulation to the point when the steering forces are stopped; that is, when the forces due to the

7388

dx.doi.org/10.1021/jp201560n |J. Phys. Chem. A 2011, 115, 7378–7391
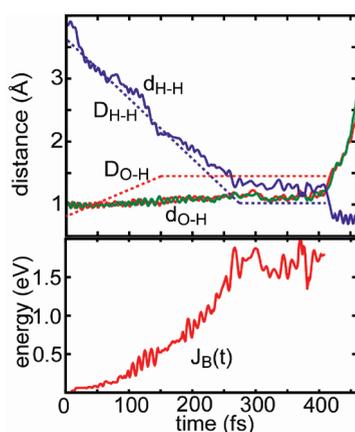
Figure 6. Steered first-principles Born—Oppenheimer molecular dynamics (SFPBOMD) simulations and the DEHE reaction. Upper panel: time variation of the functions $D_{O-H}(t)$ and $D_{H-H}(t)$ (dashed lines) appearing in the steering potentials (see Appendix B), and the time variation of the distances between the reacting H atoms, $d_{H-H}(t)$, and between the oxygen atoms of the reacting water molecules and the reacting hydrogens, $d_{O-H}(t)$, obtained from the integration of the equations of motions in the course of the SFPBOMD simulation (solid lines). The steering of the reaction is stopped at $t = 412$ fs, after which the system crosses the barrier and evolves freely (without steering). Lower panel: Integral of the work performed on the reactants bringing it to overcome the transition state activation barrier (see the integral J_B defined in Appendix B). The value of the activation barrier is equal to the value of the integral at the time when the steering of the reaction is stopped (here at $t = 412$ fs). Energy in eV, distances in Å, and time in fs.

system itself (i.e., interatomic interactions not including the steering forces) point in the direction of the reaction products (which occurred in our case at $t = 412$ fs).

The simulation described in the paper yielded an activation barrier $\Delta E_a = 1.8$ eV. Other simulations that we performed, using the same formalism but with higher O—H stretching and H—H compression rates (as well as steering beyond the bond-length values used in the simulation that we discuss) yielded much higher barriers (up to 3 eV).

In the upper panel of Figure 6 the distances d_{O-H} are shown as red and green lines, D_{O-H} is the red dashed line, d_{H-H} is in blue, and D_{H-H} is the blue dashed line. In the lower panel of Figure 6 the sum of integrated force, $J_B(t)$, is shown,

$$ J_B = \int d\tau \sum_{j \in C} f_j^C(\tau) \cdot v_j(\tau) $$

where the summation index j goes over the steered particles: $j = O_1, H_1, O_2, H_2$. In the above equation, $f_j^c(t)$ is the steering force on particle j obtained as the derivative of the steering potential with respect to the position of particle j, and $v_j(t)$ is the velocity of the particle.

◼ APPENDIX C: CLASSIFICATION AND CHARACTERI-ZATION OF THE ELECTRONIC STATES OF OH⁻ AND H₂O (FIGURE 5D)

The states of the OH⁻ anions[58] are commonly denoted by their (isolated anion) symmetries as (in order of increasing, less negative, energies) $1\sigma^2$, $2\sigma^2$ (-14.28), $3\sigma^2$ (-1.67), $1\pi^4$ (1.94), with our calculated gas-phase energies (in eV) given in

parentheses; for the electron affinity of OH, we find 1.883 eV compared to the experimentally measured value of 1.825 eV. Because of the use of pseudopotentials, the $1\sigma^2$ is not included in our calculation. The effect of hydration is to lower the energies of the states by up to 7—9 eV (see Figure 5D). The lowest energy peak of the hydrated hydroxide anion, at -21.5 eV, corresponds to the $2\sigma^2$ state, with the main binding in the ion coming from the $3\sigma^2$ state. The peak at -5 eV corresponds to the $1\pi^4$ states, which are essentially nonbinding, formed by the atomic-like p orbitals of the oxygen atom; the latter ones are those seen on the OH (though shifted in energy) in Figure 4G,H.

The states of the H_2O molecule are commonly denoted by their symmetries (of the isolated molecule) as follows:[59] $1a_1^2$ $2a_1^2$ (-25.14), $1b_2^2$ (-13.07), $3a_1^2$ (-9.27), and $1b_1^2$ (-2.19), with our calculated values for the isolated molecule given in parentheses (in eV). Through comparison of the upper and lower edges of the DOS for the neutral $(H_2O)_{103}$ cluster with that for the $(H_2O)_{103}(OH^-)_2$ cluster (Figure 5D), we have shown that charging effect in the latter, bring about an almost rigid shift of its states to higher energies by about 3 eV. Because of the use of pseudopotentials, the $1a_1^2$ state is not included in our calculation. The states of the water molecules are significantly (inhomogeneously) broadened (and, as discussed above, they are upward shifted due to charging) in the cluster. Nevertheless, the groups of states in Figure 5D (as well as in Figure 5B, red line) can be correlated with the single molecule states as follows: the lowest energy region (between -20 eV and -24 eV) corresponds to $2a_1^2$ (involving the 2s orbital of the oxygen atom) and the states in the range -9 to -12 eV correspond to $1b_2^2$ (involving the in-plane $2p_x$ orbital of the oxygen), with both these groups of states contributing to the attractive internuclear force in H_2O. The states between $-6,V$ and -9 eV correlate with $3a_1^2$ (which is less binding than the other previous two groups), and finally, the states in the range -3 and -6 eV correspond to the lone-pair of the H_2O molecule, which lies in the plane perpendicular to the molecular plane (these are the p-like states seen in Figures 5C for the water molecules located at the surface of the cluster (because of reduced hydrogen bonding, their orbital energies lie at the top of the electronic spectrum).

◼ APPENDIX D: PERTINENT DETAILS ABOUT THE CLASSICAL MD SIMULATIONS (FIGURE 4I)

Starting at the end of the FPBOMD simulation (configuration H in Figure 4), we performed a 30 ps classical MD simulation of the $(H_2O)_{103}(OH^-)_2$ at 250 K for the interaction potentials used, see below. This was followed by a cooling MD simulation (employing stochastic temperature control, see ref 41) to 50 K over a 12 ps time interval, culminating with structural optimization and subsequent dynamical evolution at 50 K via a FPBOMD simulation for an additional 1 ps time interval.

In classical molecular dynamics simulations of the water cluster, we employed the TIP3P model potentials,[55] as implemented in the CHARMM force field.[56] The difference from the original TIP3P potentials lies in the Lennard-Jones potentials where, unlike the original TIP3P model potential, the CHARMM version places Lennard-Jones potentials on the hydrogen atoms, in addition to the ones on the oxygen atoms. The partial charges of the TIP3P model are not modified.[56]

The hydroxide potential used in simulations of the $(H_2O)_{103}(OH^-)_2$ cluster was constructed from the CHARMM/TIP3P water potential by removing one of the hydrogen atoms

7389

dx.doi.org/10.1021/jp201560n |J. Phys. Chem. A 2011, 115, 7378–7391

and increasing the negative point charge on the oxygen so that the total charge on it is −1e. The Lennard-Jones and OH stretch terms were unchanged. With these modifications, we obtain the "4 + 1" coordination of the hydroxide anions with reduced O−O distances between the oxygen atom of the hydroxide anions and the oxygen atoms of the neighboring water molecules, as predicted by previous MD simulations[50b] and deduced from recent experiments.[60]

■ **AUTHOR INFORMATION**

Corresponding Author

*E-mail: uzi.landman@physics.gatech.edu.

■ **REFERENCES**

(1) Weyl, W. *Pogg. Ann* **1864**, *123*, 350.

(2) Symons, M. C. R. *Chem. Soc. Rev.* **1976**, *5*, 337.

(3) Hart, E. J.; Boag, J. W. *J. Am. Chem. Soc.* **1962**, *84*, 4090.

(4) Hart, E. J.; Anbar, M. *The Hydrated Electron*; Wiley: New York, 1970.

(5) Neumark, D. M. *Mol. Phys.* **2008**, *100*, 2183.

(6) Coe, J. V.; Williams, S. M.; Bowen, K. H. *Int. Rev. Phys. Chem.* **2008**, *27*, 27.

(7) Armbruster, M.; Haberland, H.; Schindler, H. −G. *Phys. Rev. Lett.* **1981**, *47*, 323.

(8) Haberland, H.; Ludewight, C.; Schindler, H. G.; Worsnop, D. R. *J. Chem. Phys.* **1984**, *81*, 3742.

(9) (a) Knapp, M.; Echt, O.; Kreisle, D.; Recknagel, E. *J. Chem. Phys.* **1986**, *85*, 636.(b) *J. Phys. Chem.*, **1987**, *91*, 2601.

(10) Coe, J. V.; Lee, G. H.; Eaton, G.; Arnold, S. T.; Sarkas, H. W.; Bowen, K. H.; Ludewigt, C.; Haberland, H.; Worsnop, D. R. *J. Chem. Phys.* **1990**, *92*, 3980.

(11) (a) Barnett, R. N.; Landman, U.; Cleveland, C. L.; Jortner, J. *J. Chem. Phys.* **1988**, *88*, 4421.(b) *ibid.* **1988**, *88*, 4429. (c) Barnett, R. N.; Landman, U.; Cleveland, C. L.; Jortner, J. *Phys. Rev. Lett.* **1987**, *59*, 811. (d) Barnett, R. N.; Landman, U.; Nitzan, A. *J. Chem. Phys.* **1989**, *91*, 5567. (e) Barnett, R. N.; Landman, U.; Nitzan, A. *Phys. Rev. Lett.* **1989**, *62*, 106.

(12) Barnett, R. N.; Landman, U.; Jortner, J. *Chem. Phys. Lett.* **1988**, *145*, 382.

(13) Kaukonen, H.-P; R.N. Barnett, R. N.; Landman, U. *J. Chem. Phys.* **1992**, *97*, 1365.

(14) (a) Ayotte, P; Johnson, M. A. *J. Chem. Phys.* **1997**, *106*, 811. (b) Ayotte, P; Weddle, G. H.; Bailey, C. G.; Johnson, M. A.; Vila, F.; Jordan, K. D. *J. Chem. Phys.* **1999**, *110*, 6268.

(15) Paik, D. H.; Lee, I.; Yang, D. S.; Bakin, J. S.; Zewail, A. H. *Science* **2004**, *306*, 672.

(16) (a) Asmis, K. R.; Santambrogio, G.; Zhou, J.; Garand, E.; Headrick, J.; Goebbert, D.; Johnson, M. A.; Neumark, D. M. *J. Chem. Phys.* **2007**, *126*, 191105. (b) Verlet, J. R. R.; Bragg, A. E.; Kammrath, A.; Cheshnovsky, O.; Neumark, D. M. *Science* **2005**, *307*, 93. (c) Verlet, J. R. R.; Bragg, A. E.; Kammrath, A.; Cheshnovsky, O.; Neumark, D. M. *Science* **2005**, *310*, 1769. (d) Bragg, A. E.; Verlet, J. R. R.; Kammrath, A.; Cheshnovsky, O.; Neumark, D. M. *J. Am. Chem. Soc.* **2005**, *127*, 15283.

(e) Kammrath, A.; Verlet, J. R. R.; Griffin, G. B.; Neumark, D. M. *J. Chem. Phys.* **2006**, *125*, 076101.

(17) Ma, L.; Majer, K.; Chirot, F.; von Issendorff, B. *J. Chem. Phys.* **2009**, *131*, 144303.

(18) (a) Turi, I.; Sheu, W.-S.; Rossky, P. J. *Science* **2005**, *309*, 914. (b) Turi, I.; Sheu, W.-S.; Rossky, P. J. *Science* **2005**, *310*, 1769. (c) Madarasz, A.; Rossky, P.J.; Turi, L. *J. Chem. Phys. A* **2010**, *114*, 2331.

(19) (a) Forck, R. M.; Dauster, I.; Schieweck, Y; Zeuch, T.; Buck, U.; Oncak, M.; Slavicek, P. *J. Chem. Phys.* **2010**, *132*, 221102. (b) Siefermann, K. R.; Liu, Y.; Lugovoy, E.; Link, O.; Faubel, M.; Buck, U.; Winter, B.; Abel, B. *Nature Chem.* **2010**, *2*, 274.

(20) (a) Marsalek, O.; Uhlig, F.; Frigato, T.; Schnidt, B.; Jungwirth, P. *Phys. Rev. Lett.* **2010**, *105*, 043002. (b) Frigato, T.; VandeVondele, J.; Schmidt, B.; Schutte, C.; Jungwirth, P. *J. Chem. Phys. A* **2008**, *112*, 6125.

(21) Makov, G.; Nitzan, A. *J. Chem. Phys.* **1994**, *98*, 3459.

(22) Ferradini, C.; Jay-Gerin, J.-P. *Radiat. Phys. Chem.* **1993**, *41*, 487.

(23) Basco, N.; Kenney-Wallace, G. A.; Vidyarthi, S. K.; Walker, D. C. *Can. J. Chem.* **1972**, *50*, 2059.

(24) (a) Han, P.; Bartels, D. M. *J. Phys. Chem.* **1992**, *96*, 4900. (b) Schmidt, K. H.; Bartels, D. M. *Chem. Phys.* **1995**, *190*, 145.

(25) Weiss, J., J. *Nature* **1960**, *186*, 751.

(26) Rabani, J.; Stein, G. *J. Chem. Phys.* **1962**, *37*, 1865.

(27) Dorfman, L. M.; Taub, I. *J. Am. Chem. Soc.* **1963**, *85*, 2370.

(28) Meisel, D.; Czapski, G.; Matheson, M. S.; Mullac, W. A. *Int. J. Rad. Phys. Chem.* **1975**, *7*, 233.

(29) Copeland, D. A.; Kestner, N. R. *J. Chem. Phys.* **1973**, *58*, 3500.

(30) Feng, D. F.; Fueki, K.; Kevan, L. *J. Chem. Phys.* **1973**, *58*, 3281.

(31) (a) Larsen, R. E.; Schwartz, B. *J. Phys. Chem. B* **2004**, *108*, 11760.(b) *ibid.* **2006**, *110*, 1006. (c) *ibid.* **2006**, *110*, 9681.

(32) Fois, E. S.; Selloni, A.; Parrinello, M.; Car, R. *J. Phys. Chem.* **1988**, *92*, 3268.

(33) Rajagopal, G.; Barnett, R. N.; Nitzan, A.; Landman, U.; Honea, E.; Labastie, P.; Homer, M. L.; Whetten, R. L. *Phys. Rev. Lett.* **1990**, *64*, 2933.

(34) Rajagopal, G.; Barnett, R. N.; Landman, U. *Phys. Rev. Lett.* **1991**, *67*, 727.

(35) (a) Hakkinen, H.; Barnett, R. N.; Landman, U. *Europhys. Lett.* **1994**, *28*, 263. (b) Hakkinen, H.; Barnett, R. N.; Landman, U. *Chem. Phys. Lett.* **1995**, *232*, 79. (c) Barnett, R. N.; Cheng, H.-P.; Hakkinen, H.; Landman, U. *J. Phys. Chem.* **1995**, *99*, 7731.

(36) Zhang, L; Yan, S.; Cukier, R. I.; Bu, Y. *J. Phys. Chem. B* **2008**, *112*, 3767.

(37) (a) Thompson, J. C. *Electrons in Liquid Ammonia*; Oxford University Press: London, 1976. (b) Mott, N. F. *Metal−Insulator Transition*; Barnes and Noble: New York, 1974. (c) Mott, N. F. *J. Phys. Chem.* **1975**, *79*, 2915. (d) Deng, Z. H.; Martyna, G. J.; Klein, M. L. *Phys. Rev. Lett.* **1992**, *68*, 2496.(f) *ibid.* **1993**, *71*, 267. (g) *J. Chem. Phys.* **1994**, *100*, 7590. (e) Martyna, G. J.; Deng, Z. H.; Klein, M. L. *J. Chem. Phys.* **1993**, *98*, 555.

(38) Even, U.; Jortner, J.; Noy, D.; Lavie, N.; Cossart-Magos, C. *J. Chem. Phys.* **2000**, *112*, 8068.

(39) J. Zhang, J.; Enke, C. G. *J. Am. Soc. Mass Spectrom.* **2000**, *11*, 759.

(40) Alternative decay channels of the doubly-charged clusters include (i) single electron emission (note the calculated low values for the first vertical detachment energies), VDE(1), and (ii) the DEHE reaction on which we focus in this study.

(41) Barnett, R. N.; Landman, U. *Phys. Rev. B* **1993**, *48*, 2081.

(42) Trouillier, N.; Martins, J. L. *Phys. Rev. B* **1991**, *43*, 1993.

(43) Perdew, J. P.; Burke, K.; Ernzerhof, M. *Phys. Rev. Lett.* **1996**, *77*, 3865.

(44) Barnett, R. N.; Landman, U. *J. Phys. Chem.* **1995**, *99*, 17305.

(45) Cheng, H.P-.; Barnett, R. N.; Landman, U. *Chem. Phys. Lett.* **1995**, *237*, 161.

(46) Sim, F.; St-Amant, A.; Papal, I.; Salahub, D. R. *J. Am. Chem. Soc.* **1992**, *114*, 4391.

(47) Barnett, R. N.; Landman, U., manuscript in preparation.

(48) To account for the estimated experimental thermal conditions (that is, several tens of degrees Kelvin, see Experimental Section), the information that we give for the singly- and doubly-charged clusters (see text and Figure 3) was obtained from simulations where in the final stage of preparation (for details, see Appendix A) the clusters were cooled to 50 K and dynamically evolved using the FPBOMD method (see ref 41) for up to 5 ps. Simulations where the clusters were allowed to evolve at higher temperatures (200−250 K) yielded similar results pertaining to energetics (in particular, average vertical detachment energies) but with larger fluctuations and somewhat smaller radii of gyration (particularly for the singly-charged clusters); in this context, see theoretical discussions of preparation and thermal effects in refs 11d, 11e, 18c, and 20a.

(49) Other attachment modes that we have explored include (a) a higher (total) energy surface state where both electrons are bound in a common surface cavity, characterized by a very diffuse electron distribution (similar in appearance to that shown here for the one-electron diffuse sd state, see Figure 3F) with one of the excess electrons having a negative VDE and (b) an even higher (total) energy state with one electron localized internally and the other bound at the surface.

(50) (a) Tuckerman, M. E.; Marx, D.; Parrinello, M. *Nature* **2002**, *417*, 925. (b) Chen, B; Ivanov, I.; Park, J. M.; Parrinrllo, M.; Klein, M. L. *J. Phys. Chem. B* **2002**, *106*, 12006.

(51) (a) Zhan, C. G.; Dixon, D. A. *J. Phys. Chem. A* **2002**, *106*, 9737. (b) Khalack, J.; Lyubartsev, A. P. *J. Phys. Chem. A* **2005**, *109*, 378.

(52) We give here the geometrical parameters that characterize the hydroxide hydration structures, I and II, shown as insets in Figure 5D. For structure I in Figure 5D (where the O−H anion points downward, i.e., oriented as an acceptor with respect to the H_2O molecule at the apex of the pyramid), the average distance O*−O between the oxygen of the hydroxide (denoted as O*) and the oxygens of the water molecules in the base plane $\langle d(O^*{-}O)\rangle$ = 2.69 Å with a range of variation $\Delta(O^*{-}O)$ = 2.67−2.75 Å, the average distance of O* from the nearest H atom of the planar H_2O molecules is $\langle d(O^*{-}H)\rangle$ = 1.70 Å with $\Delta(O^*{-}H)$ = 1.67−1.77 Å, and the distances between the oxygens of neighboring water molecules in the base plane $\langle d(O{-}O)\rangle$ = 3.71 Å and $\Delta(O{-}O)$ = 3.14−4.35 Å. For the water molecule above the plane (whose oxygen atom we denote as O'), $d(O^*{-}O')$ = 2.78 Å and $d(O^*{-}H')$ = 1.81 Å, and $\langle d(O'{-}O)\rangle$ = 3.52 Å, $\Delta(O'{-}O)$ = 3.22−3.75 Å . For structure II (where the O−H anion is oriented as a donor with respect to the H_2O molecule at the apex of the pyramid), we find for the four water molecules in the base, $\langle d(O^*{-}O)\rangle$ = 2.68 Å, $\Delta(O^*{-}O)$ = 2.59−2.85 Å; $\langle d(O^*{-}H)\rangle$ = 1.67 Å; $\Delta(O^*{-}H)$ =1.56−1.89 Å, $\langle d(O{-}O)\rangle$ = 3.73 Å and $\Delta(O{-}O)$ = 3.31−4.13 Å, and $\langle d(O'{-}O)\rangle$ = 4.32 Å, $\Delta(O'{-}O)$ = 3.5−5.4 Å; the somewhat larger ranges of distance variations for structure II indicate some deviation from planarity (as described above), which is obvious from inspection of the shown structure. For the water molecule above the plane in structure II, we find $d(O^*{-}O')$ = 3.08 Å and $d(H^*{-}O')$ = 2.15 Å (where H* is the hydrogen atom of the hydroxide anion).

(53) (a) Friedman, H. L.; Krishnan, V. V. *Water, A Comprehensive Treatise*; Plenum: New York, 1973. (b) Zhu, T.; Li, J.; Hawkins, G. D.; Cramer, C. J.; Truhlar, D. G. *J. Chem. Phys.* **1998**, *109*, 9177.

(54) In the equilibrated $(H_2O)_{103}(OH^-)_2$ cluster, the hydrated hydroxide anions are found preferentially in the surface region, in the sense that some of the H_2O molecules in the hydration shell of the hydroxides are found to be undercoordinated (i.e., miss neighbors) because of the proximity to the surface; for a review of recent developments pertaining to the issue concerning preferential segregation of hydroxide ions at the surface of water, see *Chem. Eng. News*, **2010**, *88* (28), 35. For reference, we recall that in the bulk a fully coordinated water molecule would have 2 H-donor and 2 H-acceptor neighboring molecules. Analysis of the cluster configuration shown in Figure 5C reveals that for one of the hydroxides (the one of the left) two of the H_2O in its first hydration shell miss (each) an H-acceptor molecule and one of its hydrating H_2O misses both an H-donor and an H-acceptor molecules, and for the other hydroxide, we find that three of its hydrating H_2O miss (each) an H-acceptor molecule.

(55) Jorgensen, W. L.; Chandrasekhar, J.; Madura, J. D.; Impey, R. W.; Klein, M. L. *J. Chem. Phys.* **1983**, *79*, 926.

(56) MacKerell, A. D., Jr.; Bashford, D.; Bellott, R. L.; Dunbrack, R. L., Jr.; Evanseck, J. D.; Field, M. J.; Fischer, S.; Gao, J.; Guo, K.; Ha, S.; Joseph-McCarthy, D.; Kuchnir, L.; Kuczera, K.; Lau, F. T. K.; Mattos, C.; Michnick, S.; Ngo, T.; Nguyen, D. T.; Prodhom, B.; Reiher, W. E., III; Roux, B.; Schlenkrich, M.; Smith, J. C.; Stote, R.; Straub, J.; Watanabe, M.; Wiorkiewicz-Kuczera, J.; Yin, D.; Karplus, M. *J. Phys. Chem.* **1998**, *102*, 3586.

(57) Cornell, W. D.; Cieplak, P.; C.I. Bayly, C. I.; Gould, I. R.; Merz, K. M.; Ferguson, D. M.; Spellmeyer, D. C.; Fox, T.; Caldwell, J. W.; Kollman, P. A. *J. Am. Chem. Soc.* **1996**, *118*, 2309.

(58) Bader, Q. F. W.; Keaveny, I. *J. Chem. Phys.* **1967**, *47*, 3381.

(59) Pitzer, R. M.; Aung, S.; Chan, S. I. *J. Chem. Phys.* **1968**, *49*, 2071.)

(60) Megyes, T.; Balint, S.; Grosz, T.; Radnai, T.; Bako, I.; Sipos, P. *J. Chem. Phys.* **2008**, *128*, 044501.